HHS Public Access

Author manuscript

Neurobiol Dis. Author manuscript; available in PMC 2017 October 01.

Published in final edited form as:

Neurobiol Dis. 2016 October ; 94: 18–31. doi:10.1016/j.nbd.2016.05.016.

Pathological conformations involving the amino terminus of tau occur early in Alzheimer's disease and are differentially detected by monoclonal antibodies

Benjamin Combs[a], **Chelsey Hamel**[a], and **Nicholas M. Kanaan**[a,b,c,*]

Benjamin Combs: Benjamin.Combs@hc.msu.edu; Chelsey Hamel: Chelsey.Hamel@hc.msu.edu; Nicholas M. Kanaan: Nicholas.Kanaan@hc.msu.edu

[a]Department of Translational Science and Molecular Medicine, College of Human Medicine, Michigan State University, 333 Bostwick Ave NE, Grand Rapids, MI 49503, USA

[b]Neuroscience Program, Michigan State University, 333 Bostwick Ave NE, Grand Rapids, MI 49503, USA

[c]Hauenstein Neuroscience Center, Mercy Health Saint Mary's, 220 Cherry St SE, Grand Rapids, MI 49503, USA

Abstract

Conformational changes involving the amino terminus of the tau protein are among the earliest alterations associated with tau pathology in Alzheimer's disease and other tauopathies. This region of tau contains a phosphatase-activating domain (PAD) that is aberrantly exposed in pathological forms of the protein, an event that is associated with disruptions in anterograde fast axonal transport. We utilized four antibodies that recognize the amino terminus of tau, TNT1, TNT2 (a novel antibody), Tau12, and Tau13, to further study this important region. Using scanning alanine mutations in recombinant tau proteins, we refined the epitopes of each antibody. We examined the antibodies' relative abilities to specifically label pathological tau in non-denaturing and denaturing assays to gain insight into some of the mechanistic details of PAD exposure. We then determined the pattern of tau pathology labeled by each antibody in human hippocampal sections at various disease stages in order to characterize PAD exposure in the context of disease progression. The characteristics of reactivity for the antibodies fell into two groups. TNT1 and TNT2 recognized epitopes within amino acids 7–12 and specifically identified recombinant tau aggregates and pathological tau from Alzheimer's disease brains in a conformation-dependent manner. These antibodies labeled early pre-tangle pathology from neurons in early Braak stages and colocalized with thiazine red, a marker of fibrillar pathology, in classic neurofibrillary tangles. However, late tangles were negative for TNT1 and TNT2 indicating a loss of the epitope in later stages of tangle evolution. In contrast, Tau12 and Tau13 both identified discontinuous epitopes in the amino

*Corresponding author at: Department of Translational Science and Molecular Medicine, College of Human Medicine, Michigan State University, 333 Bostwick Ave NE, Grand Rapids, MI 49503, USA.

Conflict of interest

The authors report no conflicts of interest.

Ethical approval

All animal studies were performed in accordance with standard regulations and were approved by the Michigan State University Institutional Animal Care and Use Committee.

terminus and were unable to differentiate between normal and pathological tau in biochemical and tissue immunohistological assays. Despite the close proximity of these epitopes, the antibodies demonstrated remarkably different abilities to identify pathological changes in tau indicating that detection of conformational alterations involving PAD exposure is not achieved by all N-terminal tau antibodies and that a relatively discrete region of the N-terminus (i.e., amino acids 7–12, the TNT1 and TNT2 epitope) is central to the differences between normal and pathological tau. The appearance of PAD in early tau pathology and its disappearance in late-stage tangles suggest that toxic forms of tau are associated with the earliest forms of tau deposits. Collectively, these findings demonstrate that the TNT antibodies are useful markers for early conformational display of PAD and provide information regarding conformational changes that have potential implications in the toxic mechanisms of tau pathology.

Keywords

Tau; Alzheimer’s disease; Tauopathies; Neurodegeneration; Protein misfolding; Protein aggregation; Conformation; Antibodies

1. Introduction

Alzheimer’s disease (AD) is a neurodegenerative disorder characterized by pathological aggregation of tau protein and the amyloid-β peptide leading to the formation of intracellular neurofibrillary tangles (NFTs) and extracellular senile plaques, respectively (Braak and Braak, 1991). There is an association between tau pathology deposition and loss of cells and synapses, but a growing body of evidence suggests that NFTs may not be the cause of neurotoxicity (Bobinski et al., 1997; Bussiere et al., 2003; Gomez-Isla et al., 1997; Morsch et al., 1999; Santacruz et al., 2005; Spires-Jones et al., 2008; Wittmann et al., 2001; Yoshiyama et al., 2007). Therefore, it is important to understand how the early pre-tangle alterations in tau may lead to toxicity and why this toxicity is apparently lost or reduced in mature fibrillar pathology.

Changes in tau conformation may play an important role in the development of early tau pathology and tau-mediated toxicity. Tau is traditionally described as a disordered protein; however, evidence suggests that tau proteins fold into multiple conformations. Initial evidence of tau folding was derived from the description of the discontinuous Alz50 and MC1 epitopes, which label otherwise normal-appearing neurons early in disease progression and prior to NFT formation (Carmel et al., 1996; Hyman et al., 1988; Jicha et al., 1999, 1997). The disease specificity of these two antibodies indicated that tau undergoes a conformational change involving a close association of the N-terminus and microtubule-binding domains in Alzheimer’s disease. More recently, a global conformation known as the global hairpin or “paperclip” conformation, where the N- and C-termini are in close proximity and the C-terminus and microtubule-binding domains are interacting, was described (Jeganathan et al., 2006). Folding of the N-terminus into this conformation is impaired by mimicking phosphorylation epitopes (e.g. the AT8 site) associated with Alzheimer’s disease (Goedert et al., 1995; Greenberg et al., 1992; Jeganathan et al., 2008; Mercken et al., 1992).

Changes in the conformations of tau are particularly important because they can directly affect the function of the protein and its toxic role in disease. One key example involves the recently identified phosphatase-activating domain (PAD) motif, seated in the extreme N-terminus of tau, whose exposure depends upon changes in tau folding (Kanaan et al., 2011). Recently, we developed a monoclonal antibody, Tau N-terminal 1 (TNT1), which identifies PAD exposure in non-denaturing assays (Kanaan et al., 2011). Evidence from the TNT1 antibody suggests that PAD is exposed in pathological forms of tau, including aggregated recombinant tau and tau from AD brains, but not monomeric recombinant tau and tau isolated from non-demented human brains (Kanaan et al., 2015, 2012, 2011). Aberrant exposure of this motif in disease-related forms of tau disrupts fast axonal transport, a process critical to neuron function and viability, through a signaling cascade involving PP1 and GSK3 (Kanaan et al., 2011; LaPointe et al., 2009). This links a direct toxic mechanism with conformational changes exposing the N-terminus of the protein and induced by pathological alterations in tau (e.g. aggregation or phosphorylation). This has shifted our focus to establishing how presentation of PAD is affected in Alzheimer's disease and its implications for progression of the disease.

In order to identify some mechanistic details of PAD exposure, we performed a detailed characterization of several N-terminal tau antibodies (TNT1, TNT2, Tau12, and Tau13) for their abilities to differentially recognize pathological, PAD-exposed tau or normal forms of the tau protein. The epitopes of these antibodies displayed distinct patterns of reactivity despite only small differences in their epitopes. The TNT1 (Kanaan et al., 2011) and TNT2 (a newly described reagent) antibodies displayed strong, conformation-dependent reactivity with pathological forms of tau, but not normal tau in non-denaturing assays. In contrast, Tau12 (Horowitz et al., 2004) and Tau13 (Ghoshal et al., 2002) did not detect differences between pathological and normal tau, demonstrating that not all N-terminal antibodies are useful for this purpose and the relevant conformational changes involve, and may be limited to, amino acids 7–12. The TNT antibodies labeled diffuse, pre-tangle pathology in hippocampal tissue sections from Braak stages I–VI cases. The TNT1 and TNT2 antibodies colocalized with pathology identified by the early, conformation-specific Alz50 antibody, and remained in classical NFTs but did not co-label in thiazine red (ThR)-positive late-stage NFTs (e.g. ghost tangles). These findings demonstrate that TNT1 and TNT2 are useful reagents to differentiate normal from pathological, PAD-exposed forms of the tau protein, and that PAD exposure is an early conformational change in tau that occurs as pathology begins to accumulate in neurons.

2. Materials and methods

2.1. Recombinant tau proteins

The full-length human tau protein construct (2N4R/hT40) containing a C-terminal 6xHis tag in the pT7 plasmid was used to produce recombinant tau protein as described (Kanaan et al., 2011). Site-directed mutagenesis (Agilent Quikchange Lightning, Santa Clara, CA, 210519-5) was used to introduce the following mutations in the hT40 construct: E3A, P4A, R5A, Q6A, E7A, FE8-9AA, V10A, M11A, E12A, D13A/H14A/A15A/G16A/T17A (X13-17A), Y18A/G19A/L20A/G21A (X18-21A), or D22A/R23A/K24A (X22-24A). In

addition, wild-type versions of the other five human tau isoform proteins (2N3R/hT39, 1N4R/hT34, 1N3R/hT37, 0N4R/hT24, and 0N3R/hT23) were produced. These constructs were transformed into T7 Express competent cells (New England Biosciences, Ipswich, MA, C2566I). 125 ml of Luria Broth was inoculated with the bacteria and grown overnight at 25 °C until it reached an OD_{600} value of 0.8–1.0. IPTG was added to the flask at a final concentration of 1 mM and incubated at 37 °C for 2 h. The cells were centrifuged at 8000 × *g* for 10 min, washed with saline buffer and centrifuged again at 8000 × *g* for 10 min. The pellet was frozen at −80 °C. The cells were resuspended in buffer (50 mM NaCl, 1 mM Tris, and 500 nM imidazole, with protease inhibitors at 10 μg/ml of pepstatin, leupeptin, bestatin, and aprotinin, and 1 mM PMSF, pH 8.0) and lysed by sonication (20 pulses of 5 s each at power setting of 3, Misonix XL-2000) on ice. Protease inhibitors were again added to the lysate at the same concentrations as above along with Brij 35 to 0.1%. The sample was then centrifuged at 107,000 × *g* for 20 min at 4 °C. Protease inhibitors and 10% glycerol were added to the supernatant before loading it onto 1 ml of Talon metal affinity resin (Clontech, Mountain View, CA, #635502). After a 20 ml buffer wash, the protein was eluted into 1 ml fractions by adding 10 ml of elution buffer (50 mM NaCl, 1 mM Tris, and 100 mM imidazole with 2 mM PMSF). The samples were analyzed by SDS-PAGE and Coomassie staining and fractions with protein were combined and dithiothreitol (DTT) was added to 1 mM final concentration.

Protein concentrations were determined by SDS Lowry where 200 μl of the proteins were added to 200 μl of SDS solution (2% SDS, 5% β-mercaptoethanol, 10% glycerol, 62.5 mM Tris, pH 6.8), respectively, along with buffer-only blank samples. Protein standards of 0, 2, 4, 8, 16, and 32 μg were generated using a 2 mg/ml bovine serum albumin (BSA) stock (Thermo Fisher Scientific, Waltham, MA, #23209) and adding SDS solution to a total volume of 100 μl. 1 ml of 10% perchloric acid/1% phosphotungstic acid was added to each sample, vortexed, and briefly spun in microcentrifuge before a 1 h incubation on ice. The samples were then centrifuged at 18,000 × *g* for 15 min at 4 °C and the supernatant was removed. After the protein pellet had completely dried, it was dissolved in 1 ml of Lowry solution (0.01% $CuSO_4$, 0.02% sodium potassium tartate, and 2% sodium carbonate in 0.1 N sodium hydroxide) and incubated at RT for 10 min. 100 μl of Folin–Ciocalteu's phenol reagent (diluted 1:1 in water, Sigma–Aldrich, St. Louis, MO, F9252) was added and incubated for 30–45 min at RT. 100 μl of each sample was added, in duplicate, to a clear 96-well plate and the absorbances were read at 750 nm. The total protein concentrations were interpolated from the BSA standard curve ($r^2 = 0.98$). The protein was aliquoted into 10–50 μl and frozen at −80 °C.

2.2. Animals

An adult male Sprague–Dawley rat (Harlan, Indianapolis, IN, 002), an adult male C57BL/6J mouse (The Jackson Laboratory, Bar Harbor, ME, 000664), and an adult male tau knockout mouse (The Jackson Laboratory, 007251) were used to obtain brain lysate samples. The animals were sacrificed approximately 7 days after delivery and were transcardially perfused with 0.9% saline with heparin (10,000 U/L) to clear the blood. The frontal cortex was microdissected and stored at −80 °C until processed for generating brain lysate samples for characterizing N-terminal antibodies (see below). All animal studies were performed in

accordance with standard regulations and were approved by the Michigan State University Institutional Animal Care and Use Committee.

2.3. Generation of the tau N-terminal 2 (TNT2) antibody

This is the first description of the novel mouse monoclonal TNT2 antibody. TNT2 was generated by immunizing mice with a peptide of amino acids 2–18 of hT40 (^{2}AEPRQEFEVMEDHAGTY ^{18}) conjugated to KLH as described (Kanaan et al., 2011). Briefly, BALB/c female mice (Jackson Laboratories, #001026) were immunized subcutaneously every 3 weeks for 5 months. After immunization, the splenocytes were fused to SP2/o myeloma cells and positive clones that reacted with PAD in indirect ELISAs (as described below) were subcloned four times. Isotype strips were used to determine that TNT2 is an IgG1. A CELLine Classic 1000 bioreactor (Sartorius AG, DC-90005) was used to produce TNT2 before purification with protein A sepharose (GE Healthcare, Little Chalfront, UK, #17-1279-02) using methods similar to those previously described (Kanaan et al., 2011). Purified TNT2 was dialyzed into antibody storage buffer (10 mM HEPES, 500 mM NaCl, 50% glycerol, pH 7.4), adjusted to 1 mg/ml, aliquoted and stored at −80 °C.

2.4. Rodent brain lysates for antibody characterization

Tissue samples from the frontal cortex of a rat, mouse, and tau knockout mouse (from above) were processed to assess the species cross-reactivity and specificity of TNT1, TNT2, Tau12, and Tau13. Tissue pieces were homogenized in 375 μl lysis buffer (0.8 M NaCl, 10% sucrose, 1 mM EDTA, 10 mM Tris, pH 7.4) containing protease inhibitors (as above) and phosphatase inhibitors (β-glycerophosphate and sodium orthovanadate at 1 mM) by sonication (power setting = 3, 20 × 5 s pulses on ice). Debris was removed by spinning samples at 12,000 × *g* for 10 min. The resulting supernatant was assessed for total protein concentration using the Bradford assay where 1, 2, 4, and 8 μl of sample were diluted to 160 μl of water. Triplicate BSA standards of 5, 10, 20, 40, and 80 μg were generated through serial dilutions from a 2 mg/ml stock. Corresponding control samples were made with lysis buffer at the same volumes as the BSA standards. 160 μl of all samples were incubated with 40 μl of dye solution for 5 min. The absorbances of 160 μl of the sample–reagent mixes were measured at 595 nm in a clear microplate. The absorbances from the buffer-only control samples were subtracted from the BSA standards and samples. Then a linear standard curve was generated from the BSA standard absorbance values ($r^2 = 0.997$). The protein concentrations of the samples were interpolated using the standard curve. Samples were stored at −80 °C until use in western blotting as described below.

2.5. Arachidonic acid-induced tau aggregation in vitro

Recombinant tau monomer and aggregate samples were generated by making a 400 μl reaction with 2 μM hT40 tau containing a C-terminal 6xHis tag in polymerization buffer (5 mM DTT, 100 mM NaCl, 100 μM EDTA, and 10 mM HEPES at pH 7.64). The reaction was split in half and 7.5 μl of 2 mM arachidonic acid in ethanol was added to a final concentration of 75 μM in order to induce tau polymerization in the aggregate sample. The monomer sample received 7.5 μl of ethanol as a control. The reactions were allowed to proceed overnight and the extent of aggregation was confirmed using right-angle laser light scattering (Gamblin et al., 2000). The aggregated tau sample produced the expected level of

light scattering (~150 a.u.). Aliquots of the samples were stored at −80 °C until used in assays outlined below.

2.6. Tau extraction from human frontal cortex tissue

Fresh frozen tissue samples from the frontal cortex of age-matched non-demented (control, n = 6) and severe AD cases (n = 6) were obtained from the Brain Bank of the Cognitive Neurology and Alzheimer's Disease Center at Northwestern University (see Supplemental Table 1 for details on human subjects). Soluble tau and sarkosyl-insoluble tau fractions were obtained as described previously (Kanaan et al., 2015). The tissue was suspended in 10 volumes of Brain Homgenization Buffer (50 mM Tris, pH 7.4, 274 mM NaCl, 5 mM KCl with pepstatin, leupeptin, bestatin, and aprotinin protease inhibitors at 10 μg/ml and PMSF at 1 mM). The tissue was homogenized with a Tissue Tearor Model 985-370 on setting #4 for 3 × 10 s then centrifuged at 27,000 × g for 20 min at 4 °C. The supernatant fraction was collected (soluble tau) and the pellet was resuspended in 5 volumes of 1X Brain Pellet Homogenization Buffer (800 mM NaCl, 10% sucrose, 10 mM Tris, pH 7.4, 1 mM EGTA, and 1 mM PMSF). The pellet was again homogenized at #4 for 3 × 10 s and spun at 27,000 × g for 20 min at 4 °C. Sarkosyl powder (to 1% final amount) was added to the supernatant and incubated for 1 h at 37 ° C. After the sarkosyl incubation, sample was spun at 200,000 × g for 1 h at 4 °C. The pellet was resuspended in 1 ml of Brain Pellet Homogenization buffer as the sarkosyl-insoluble tau fraction. An SDS Lowry protein assay was performed on the soluble tau (4 μl + 96 μl SDS solution) and insoluble tau (using 16 μl + 84 μl SDS solution) fractions, as described above, to determine total protein concentrations. The fractions were aliquoted and stored at −80 °C until used in assays outlined below.

2.7. Indirect enzyme-linked immunosorbent assays (ELISAs)

Indirect ELISAs were used to determine the relative affinities of TNT1, TNT2, Tau12, and Tau13 antibodies. Recombinant hT40 tau protein monomer was diluted to 2 ng/μl and 50 μl was added to the wells of a 96-well high-binding plate (Corning, Corning, NY, #3590), then incubated at room temperature for 1 h and washed 2× with ELISA wash buffer (100 mM boric acid, 25 mM sodium tetraborate decahydrate, 75 mM sodium chloride, 250 μM thimerosal, 0.4% BSA (Thermo Fisher Scientific, BP1600-100), and 0.1% Tween-20). The wells were blocked with 200 μl of 5% non-fat dry milk in wash buffer for 1 h and washed 2×. The primary antibodies were serially diluted in 1:2 intervals from 100 ng/ml to 48.8 pg/ml and 50 μl was added to the wells for 2 h then washed 4× with wash buffer. The wells were then incubated for 1 h with 50 μl of horseradish peroxidase (HRP)-conjugated horse anti-mouse secondary antibody (Vector Laboratories, Burlingame, CA, PI-2000) at a dilution of 1:5000, washed 4×, then developed with 50 μl of 3,3′,5,5′-tetramethylbenzidine (TMB, Sigma, T0440). The development was stopped after 5 min with 50 μl of 3.6% H_2SO_4 and absorbance was read at 450 nm. Blank wells without tau protein were used to determine background absorbance. The absorbance values were converted to percent of light absorbed (a linear scale) using the following equation, $\%A = (1 - 10^{-x})*100$, where x is the absorbance value. The data were fit to a sigmoidal dose-response curve (all $r^2 > 0.99$).

2.8. Sandwich ELISAs

Recombinant tau sandwich ELISAs were used to measure the differential reactivity of TNT1, TNT2, Tau12, or Tau13 for monomeric and aggregated tau samples in non-denaturing conditions. Capture antibodies were diluted to 1 ng/μl and 50 μl was added per well in a 96-well plate and allowed to incubate for 1 h. All incubations were carried out at room temperature and on a shaker. The wells were washed 2× in ELISA wash buffer. The wells were blocked with 200 μl of wash buffer containing 5% non-fat dry milk for 1 h and then rinsed 2× with wash buffer. The monomer and aggregated samples were serially diluted in tris buffered saline (TBS, 150 mM NaCl, 50 mM Tris, pH 7.4) from 200 nM to 12.2 pM at 1:4 intervals and 50 μl was added to the wells for 90 min then washed 4× with wash buffer. The detection antibody (R1, a pan-tau polyclonal rabbit antibody (Berry et al., 2004)) was diluted at 1:10,000 in milk and 50 μl was added to the plates for 90 min. The wells were washed 4 times and 50 μl of HRP-conjugated goat anti-rabbit (Vector Laboratories, PI-2000) detection secondary antibody was added at a 1:5000 dilution in milk for 1 h. Then the wells were washed 4× in wash buffer followed by development with 50 μl of TMB for 5–20 min, stopped with addition of 50 μl of 3.6% H_2SO_4, and absorbance was read at 450 nm and converted to %A as above. The data were fit to a sigmoidal dose–response curve.

Sandwich ELISAs were repeated as above, except where noted, with soluble and sarkosyl-insoluble tau fractions from control and AD human brain samples. All capture antibodies (TNT1, TNT2, Tau12, Tau13, and PHF1) were diluted 1:1000 from 1 mg/ml stock solutions. For the soluble tau samples, 50 μl containing 20 μg of total protein (0.4 mg/ml; diluted in borate saline buffer) was added to each well, while 50 μl containing 2.5 μg total protein was used for the sarkosyl-insoluble samples. For 1 control and 2 AD cases, the maximum sample available was 0.03 mg/ml in 50 μl of the control case and 0.016 mg/ml in 50 μl for the AD cases. The R1 tau antibody and HRP-conjugated anti-rabbit antibodies were used as above. The ELISAs were developed for 5–9 min. Since brain lysates contained unknown amounts of tau, independent indirect ELISAs with the R1 detection antibody were performed simultaneously for each capture antibody following the above indirect ELISA method. For these standard curve indirect ELISAs, recombinant hT40 tau monomer samples ranged from 0.98 to 250 ng/well and were detected with the R1 antibody. This provided a standard curve for us to interpolate the amount of tau bound by the capture antibodies in the human sample sandwich ELISAs as described in detail previously (Kanaan et al., 2015). The absorbance values from the R1 indirect ELISA standard curve values were fit to a nonlinear one-phase association equation (all $r^2 > 0.98$). The concentrations of tau detected in each of the sandwich ELISAs were interpolated from this standard curve and used for comparisons.

2.9. Western blotting

For western blots, alanine-scanning mutant recombinant protein samples, hT40 recombinant protein samples and all brain lysate samples were prepared in Laemmli buffer (final 1× composition: 20 mM Tris, pH 6.8, 2% SDS, 6% glycerol, 1% β-mercaptoethanol, 0.002% Bromophenol Blue). All samples were heated at 99 °C for 5 min and separated using Criterion TGX Precast 4–20% gels (BioRad, Hercules, CA, #567-1094 and #567-1095) in SDS-PAGE. Proteins were then transferred to BioTrace NT nitrocellulose transfer membrane (Pall Life Sciences, Port Washington, NY, #66593) at 400 mA for 50 min. For the scanning

alanine mutant protein blots, 400 ng of each protein was loaded for the TNT1, TNT2, and Tau12 blots and 100 ng of protein was loaded for the Tau13 blot. Recombinant samples, containing a C-terminal 6× histidine tag, for each of the tau isoforms (hT40, hT39, hT34, hT37, hT24, and hT23) were diluted to 0.5 μM in TBS and loaded at 20 μl for the isoform blots. The rodent brain lysate tau blots were loaded with 80 μg of total protein for the TNT1 blot and 20 μg of total protein for the TNT2, Tau12, and Tau13 blots. 187 ng of the purified recombinant tau protein monomer and aggregate samples were loaded per lane. The human frontal cortex lysates from controls ($n = 3$) and AD ($n = 3$) were loaded at 60 μg/lane of total protein for the TNT1 and TNT2 blots and 20 μg/lane for the Tau12 and Tau13 blots. After a blocking step of 1 h with 2% milk/TBS, the membranes were probed overnight at 4 °C with primary antibodies. All antibody stocks were 1 mg/ml and diluted in 2% milk/TBS. The scanning alanine mutant blots and tau isoform blots were probed with TNT1 (1:100,000), TNT2 (1:10,000), Tau12 (1:500,000), or Tau13 (1:1,000,000) then reprobed with R1 (1:20,000) to normalize the N-terminal antibody signal for the scanning alanine mutant quantitation. The rodent brain lysates were probed with TNT1 (1:100,000), TNT2 (1:25,000), Tau12 (1:500,000), or Tau13 (1:500,000) as well as for GAPDH (1:2000, Cell Signaling D16H11 XP Rb, Danvers, MA) to serve as a loading control. The Tau12 and Tau13 blots were reprobed with R1 (1:100,000) to confirm the presence of tau. The purified recombinant tau monomer and aggregate blots were probed with TNT1 (1:200,000), TNT2 (1:25,000), Tau12 (1:500,000), or Tau13 (1:500,000) and R1 (1:10,000) also was used on all blots. The human frontal cortex lysate blots were incubated with TNT1 (1:100,000), TNT2 (1:10,000), Tau12 (1:500,000), or Tau13 (1:500,000) and also probed for GAPDH (1:2000, Cell Signaling D16H11 XP Rb,) as the loading control to normalize N-terminal tau signals. Blots were rinsed with 0.1% Tween20/TBS and then incubated with appropriate secondary antibodies diluted 1:20,000 in milk/TBS (IRDye 680RD goat anti-mouse IgG (H + L), #926-68070; and IRDye 800CW goat anti-rabbit IgG (H + L), #926-32211; both from Li-Cor Bisciences, Lincoln, NE). Blots were imaged using a Li-Cor Odyssey infrared imaging system in the 700 and 800 nm channels at 42 μm resolution. Signal intensity of bands was quantified using Li-Cor ImageStudioLite 5.2 Software. The scanning alanine mutant blot signals were normalized to R1. Three replicates of recombinant monomer and aggregated hT40 were quantified and normalized to R1 signal. The signals from the human frontal cortex control and AD samples were quantified and normalized to GAPDH signals.

2.10. Human tissue immunohistochemistry (IHC)

Hippocampal sections from control (Braak I–II, $n = 3$), mild AD (Braak III–IV, $n = 3$), and severe AD (Braak V–VI, $n = 3$) cases from the Brain Bank of the Cognitive Neurology and Alzheimer's Disease Center at Northwestern University (see Supplemental Table 1 for details on human subjects) were used to evaluate the pattern of IHC staining with TNT1, TNT2, Tau12, Tau13, and PHF1 using established methods (Kanaan et al., 2012, 2011). Wash steps were performed 6× for 10 min in 0.1% Triton-X/TBS between all steps in the procedure. The tissue was washed and then incubated in 3% hydrogen peroxide to quench endogenous peroxidase activity for 1 h at RT. The tissue was then blocked in blocking buffer (10% goat serum/2% BSA/0.4% Triton-X in TBS) followed by incubation in the primary antibody (diluted in 2% goat serum/0.1% Triton-X/TBS) overnight at 4 °C. The following dilutions from 1 mg/ml stocks were used: TNT1 1:350,000, TNT2 1:200,000, Tau12

1:450,000, Tau13 1:450,000, PHF1 1:20,000. Initial titering experiments ensured that all antibodies were used at optimal dilutions. The following day, the tissue was incubated with a biotinylated goat anti-mouse IgG (H + L) secondary antibody (Vector Laboratories, BA-9200) diluted 1:500 in 2% goat serum/0.1% Triton-X/TBS for 2 h at RT. Then the tissue was incubated in ABC solution (1 drop of solutions A and B/10 ml, Vector Laboratories, PK-6100) for 1 h at RT followed by development in 0.05% 3,3′-diaminobenzidine (DAB), 0.003% hydrogen peroxide, 0.1% Triton-X/TBS for 8 min. After development, the tissue was mounted and coverslipped with Cytoseal 60 mounting media (Thermo Fisher Scientific, #8310-16). Tissue sections from each case were processed simultaneously for each antibody staining to reduce variability between staining runs. Omission of primary antibody was run to ensure that the specificity of the IHC signal was due to tau antibody reactivity, and as expected, no signal was observed with antibody omission (data not shown) as noted previously (Kanaan et al., 2015).

2.11. Human tissue IHC quantitation

Tissue sections were imaged at 20× magnification. A reticle (750 × 750 μm) was used to analyze regions in the CA1/CA2 pyramidal neuron layer of each case (total area = 2.8–4.5 mm^2). Neurons inside of the region were counted and sorted into groups based on established criteria of the progressive patterns of tau deposition/aggregation in neurons during pathology evolution (Bancher et al., 1989, 1991; Braak et al., 1994). Here we used the terminology of Braak and colleagues (Braak et al., 1994). Examples of each group are found in Fig. 5 and Supplemental Fig. 3. Neurons staining with a pattern of diffuse, granular cytoplasmic tau pathology, often extending far into the processes, were classified as group 1 cells. Group 2 neurons displayed a combination of granular cytoplasmic pathology and compact inclusions that were rod-like and globular in morphology, along with reduced reactivity in processes. Group 3 neurons were the compact, classic flame-shaped NFTs in the somatodendritic compartment and the cells no longer had reactivity in the distal end of the processes. Neurons beyond this phenotype (e.g. group 4 or ghost tangles, the extracellular remains of neurons that once contained NFTs and that no longer have nuclei) were not readily apparent, which was confirmed with the immunofluorescence studies described below. The total cell density was used as the main comparison across disease stages, and to further determine the relative amount of the different phenotypes (i.e., group 1–3 cells) identified by each antibody, the counts for each phenotype were converted to percent of the total cells labeled for each individual case and the mean values were compared across disease stages.

2.12. Human tissue immunofluorescence (IF)

Human hippocampal sections (all of the same cases as in IHC) were co-stained using combinations of markers to confirm whether TNT antibodies colocalize with early and late tau pathology. The first series of sections were triple stained with TNT1, TNT2 or PHF1, ThR, and DAPI. ThR (Sigma–Aldrich, S570435) is a marker for β-pleated sheet protein structure associated with mature tau fibrils (Mena et al., 1995), and stored at −20 °C as a 1% stock solution (diluted in dH_2O). DAPI, a nuclear marker (Kapuscinski, 1995), was stored as a stock solution of 5 mg/ml in DMSO and frozen at −20 °C. The tissue was washed between steps and blocked as above. Primary antibodies were diluted in 2% goat serum/0.1% Triton-

X/TBS from 1 mg/ml stocks: TNT1 1:15,000, TNT2 1:15,000, or PHF1 1:3000. Initial titering experiments ensured all antibodies were used at optimal dilutions. Then the tissue was incubated in secondary antibody (AlexaFluor goat anti-mouse IgG (H + L) 488; 1:500; Invitrogen, Carlsbad, CA, #A-11001) for 2 h at room temperature. The first wash after secondary contained DAPI at a final concentration of 0.5 ng/μl. After the remaining washes, the tissue was rinsed in deionized water for 2 × 3 min then incubated in 0.004% ThR/d$H_2$0 for 20 min before 2 × 3 min washes in water. After mounting, autofluorescence was blocked by equilibrating in 70% ethanol for 2 min, incubating in 2% sudan black B, 70% ethanol for 4 min, briefly rinsed 3× in 70% ethanol, and washed in water 2 × 3 min. The slides were coverslipped with Vectashield aqueous mounting media (Vector laboratories, H-1000).

A second series of sections was quadruple labeled for TNT1 or TNT2, Alz50, ThR, and DAPI using the same protocol as above with the following primary antibody dilutions from 1 mg/ml stocks: TNT1 1:10,000 and TNT2 1:10,000. The Alz50 antibody, which identifies a discontinuous epitope related to an altered conformation that occurs early during pathological accumulation of tau (Carmel et al., 1996; Hyman et al., 1988; Jicha et al., 1997), was diluted 1:1000 from a 5.7 mg/ml stock. AlexaFluor goat anti-mouse IgM 647 (1:500; Invitrogen, #A-21238) was included with an AlexaFluor goat anti-mouse IgG1 488 (1:500; Invitrogen, #A-21121).

All IF-stained tissue was imaged using a Nikon A1+ scanning confocal microscope system equipped with 405, 488, 541, and 640 laser lines and 425–475 nm (DAPI), 500–500 nm (AlexFluor 488), 570–620 nm (ThR), 663–738 (Alz50) emission filter sets. Z-stacks were acquired at 0.5 μm step sizes and images for figures were generated by using the maximum intensity projections. Control sections were performed by omitting a single component (TNT1 antibody, TNT2 antibody, ThR, or Alz50 antibody), and as expected, each signal was specific for the appropriate marker (data not shown) as previously observed (Kanaan et al., 2015).

3. Statistical analysis

All curve fitting and statistical analyses were performed using GraphPad Prism 6 software. The recombinant hT40 western blot data were compared using a paired *t*-test (with pairs made from the same reaction mix as described above). The tau concentration values calculated from the human frontal cortex lysate ELISAs (described above) were compared using an unpaired *t*-test. The human frontal cortex lysate western blot quantitative values were compared using an unpaired *t*-test. The total cell density data and percentage of cell phenotype data were analyzed for correlations with advancing Braak stage using the Spearman rank correlation test. All tests were two-tailed with significance set at $p < 0.05$.

4. Results

4.1. Antibody epitopes map to similar but distinct areas

We used a series of alanine mutant hT40 proteins (between amino acids 2–24) to further refine the epitopes of each antibody (Fig. 1A) beyond the previously reported epitopes (all within the first 24 amino acids of tau). Mutation of amino acids 7–12 eliminated TNT1 and

TNT2 reactivity, but in general, TNT2 appeared less effective in western blots than TNT1, as indicated by the lower R1 normalized signal values (Fig. 1A–C). It is noteworthy that deletion of amino acids 2–18 did not prohibit R1 binding confirming that this polyclonal contains epitopes outside of the extreme amino terminus (Berry et al., 2004) and suggests N-terminal antibody labeling will not block R1 binding (Fig. 1A). The epitope map for both Tau12 and Tau13 displayed quite different patterns of reactivity compared to TNT1 and TNT2 (Fig. 1F). Both antibodies appeared to identify a discontinuous epitope because reactivity was substantially reduced or eliminated in the X8-9A, X13-17A, and X18-21A mutation proteins (Fig. 1D, E). Notably, none of the alanine modifications completely eliminated Tau13 reactivity but the antibody did not react with the Δ;2–18 tau protein (deletion of amino acids 2–18) suggesting some reliance on the presence of these amino acids even though the alanine mutations alone were insufficient to completely disrupt binding. Each antibody's binding affinity was identified using an indirect ELISA with full-length tau protein (Fig. 1G). All of the monoclonal N-terminal antibodies tested here are very high-affinity reagents. TNT1 reached half of the binding saturation at 4.86 ng/ml (32.4 pM) and TNT2 at 9.21 ng/ml (61.4 pM). Tau13 demonstrated the strongest affinity for tau, reaching half of its binding saturation at 2.51 ng/ml (16.73 pM) while Tau12 bound half of its maximum at 3.27 ng/ml (21.8 pM). All N-terminal antibodies were specific to tau (i.e., no reactivity with tau knockout lysates) and both TNT antibodies labeled human and rodent tau, while Tau12 and Tau13 were human specific (Supp. Fig 1).

4.2. TNT1 and TNT2 preferentially bind aggregated tau and binding is conformation dependent

Next, we measured the abilities of each antibody to detect pathological aggregated forms of tau in a non-denaturing sandwich ELISA. Varying concentrations of monomeric and aggregated full-length recombinant tau protein were incubated with each of the antibodies. The TNT1 and TNT2 antibodies did not capture detectable levels of monomeric tau (TNT1 and TNT2: EC_{50} = undetermined) except at 200 nM (9.3 ng/μl or 467 ng/well), the highest concentration tested (Fig. 2A and B). In contrast, robust reactivity was seen with aggregated tau at much lower concentrations (TNT1: EC_{50} = 6.0 nM; TNT2: EC_{50} = 2.6 nM), indicating a clear difference in reactivity between the two states of the tau proteins. Tau12 reacted well with monomeric tau (EC_{50} = 6.9 nM) and aggregated tau (EC_{50} = 2.5 nM), but the preference for aggregated over monomeric tau was less robust compared to the TNT antibodies (Fig. 2C). Tau13 demonstrated very similar affinities for tau monomers (EC_{50} = 1.9 nM) and aggregates (EC_{50} = 1.1 nM) (Fig. 2D). The conformation-dependent nature of reactivity with these N-terminal antibodies was confirmed by denaturing the same tau samples used in the ELISAs with SDS, a reducing agent, and heat exposure before immunoblotting. All of the antibodies bound equally well to monomer and aggregated tau samples in a denatured state (Fig. 2E–F).

4.3. TNT1 and TNT2 display conformation-dependent recognition of pathological tau from Alzheimer's disease brain lysates

Soluble and sarkosyl-insoluble tau fractions from the frontal cortex of age-matched controls and Alzheimer's disease cases were used in TNT1, TNT2, Tau12, Tau13, and PHF1 non-denaturing sandwich ELISAs to determine the antibodies' abilities to identify aggregated

and soluble pathological forms of tau from the human brain. In the soluble tau fraction, the TNT1 and TNT2 antibodies detected significantly more soluble tau in the Alzheimer's disease brain lysates compared to the control samples (Fig. 3A). In contrast, Tau12 and Tau13 reacted equally as well to tau in the control and Alzheimer's disease samples. PHF1 was included for its ability to specifically identify pathological forms of tau and, like TNT1 and TNT2, its signal was significantly greater in samples from Alzheimer's disease cases when compared to age-matched controls. Next, the sarkosyl-insoluble fractions were assayed in the sandwich ELISAs with each antibody. All of the tested antibodies detected significantly more insoluble tau from the Alzheimer's disease cases when compared to control cases (Fig. 3B). Finally, the conformation dependence of reactivity for TNT1, TNT2, Tau12, and Tau13 was confirmed using denaturing western blots of the soluble tau samples from three of the same control and Alzheimer's disease cases. All of the antibodies displayed similar recognition of tau from the control and Alzheimer's disease brain lysates in denaturing conditions (Fig. 3C–D). The signal intensities were normalized to GAPDH signals to account for any differences in sample loading. This is in direct contrast to the non-denaturing ELISAs where TNT1 and TNT2 had dramatically stronger reactivity to tau in Alzheimer's disease lysates compared to control lysates (Fig. 3A–B). The pan-tau antibody, R1, was used to confirm similar levels of tau that were present in control and Alzheimer's disease samples. The normalized intensities associated with Tau12 and Tau13 were much higher than those of TNT1 and TNT2 even though less total lysate was loaded indicating better performance in denaturing western blots. The relatively weak labeling by TNT1 and TNT2 in human sample western blotting may appear to suggest they do not recognize all tau isoforms. We used western blotting to probe recombinant tau isoform proteins (hT40, hT39, hT34, hT37, hT24, and hT23) with TNT1, TNT2, Tau12. and Tau13 to address this concern. Each of these N-terminal antibodies labeled all six human isoforms (Supp. Fig. 2).

4.4. N-terminal antibodies label tau pathology throughout the progression of Alzheimer's disease

Next, we aimed to establish the pattern of tau pathology labeled by each N-terminal antibody and PHF1 in human hippocampal brain slices from Braak stages I–II, II–IV, and V–VI cases. TNT1, TNT2, Tau12, Tau13, and PHF1 labeled the typical forms of Alzheimer's disease tau pathology, including NFTs, neuropil threads, and neuritic plaques (Fig. 4A–O). As expected, the total number of cells containing TNT1, TNT2, Tau12, Tau13, and PHF1 showed strong positive correlations with advancing Braak stage (Fig. 4P, see figure legend for statistics). One distinct difference between the TNT antibodies and Tau12 or Tau13 was the extent of parenchymal tau labeled. TNT1 (Fig. 4A, F, K) and TNT2 (Fig. 4B, G, L) label little to no parenchymal tau, while both Tau12 (Fig. 4C, H, M) and Tau13 (Fig. 4D, I, N) robustly label parenchymal tau, which is presumably non-pathological or normal tau within the tissue. Similar to the TNT antibodies, PHF1 did not readily label parenchymal tau (Fig. 4E, J, O).

We quantified neurons of specific tau pathology phenotypes based on established criteria describing neurons as group 1 (early pre-tangles, Fig. 5A), group 2 (intermediate tangles, Fig. 5B), and group 3 (classic mature tangles, Fig. 5C) (Braak et al., 1994). Additional representative high-magnification images of neurons from groups 1–3 (taken from a Braak

stage III–IV case) are displayed in Supplemental Fig. 3. The data are presented as a percentage of the total cells to compare changes in the proportion of each phenotype across the Braak stages (Fig. 5D–H). The percentage of TNT1-, TNT2-, Tau12-, Tau13-, and PHF1-positive group 1 neurons showed strong, significant negative correlations with Braak stages, while group 3 cells showed a strong, significant positive correlation with increasing Braak stage (Table 1). None of the group 2 cells were significantly correlated with Braak stage, except PHF1 group 2 neurons, which showed a strong, significant negative correlation (Table 1).

The majority of TNT1-positive cells were group 1 (59%) and 2 (41%) cells compared to group 3 (0.5%) cells in Braak stage I–II cases (Fig. 5D). In Braak III–IV cases, TNT1 labeled similar but decreasing proportions of each phenotype (group 1: 42%, group 2: 33%, group 3: 25%), while the majority were group 3 cells (55%) when compared to group 1 (21%) and 2 (24%) cells in Braak V–VI cases. Similarly, TNT2 primarily labeled group 1 (57%) and group 2 (29%) cells compared to group 3 (15%) cells in Braak I–II cases, while similar amounts of each phenotype were labeled (group 1: 42%, group 2: 27%, group 3: 31%) in Braak III–IV cases (Fig. 5E). In Braak V–VI cases, the majority were group 3 cells (group 1: 32%, group 2: 29%, group 3: 39%). Tau12 labeled more group 1 cells (58%) compared to group 2 (33%) and group 3 cells (10%) in Braak I–II cases (Fig. 5F). The antibody labeled more group 3 cells (51%) compared to groups 1 (21%) and 2 (28%) cells in Braak III–IV and more group 3 cells (52%) compared to group 1 (19%) and 2 (30%) cells in Braak V–VI cases as well. Tau13 labeled more group 1 cells (72%) compared to group 2 (28%) and 3 cells (0.6%) in Braak I–II cases (Fig. 5G). Similar proportions of each phenotype (group 1: 29%, group 2: 40%, group 3: 31%) were identified with Tau13 in Braak III–IV cases, while in Braak V–VI cases, more group 3 cells (55%) were labeled when compared to group 1 (15%) and 2 (30%) cells. PHF1 stained similar amounts of all three cell phenotypes in Braak I–II (group 1: 28%, group 2: 45%, group 3: 26%) and mostly group 3 cells (48%) in Braak stages III–IV cases (group 1: 22%, group 2: 31%, Fig. 5H). There was a robust shift in the proportion of PHF1-labeled group 3 cells (89%) when compared to group 1 (2%) and 2 (9%) cells in Braak stage V–VI cases.

4.5. PAD is exposed in early tau pathology but not late-stage tangles

We performed a series of immunofluorescence co-labeling experiments with TNT1 or TNT2 and ThR, and qualitative evaluations of sections (using the same cases as in IHC) were performed to identify the different cell phenotypes and to confirm whether TNT1 and TNT2 recognize PAD exposure in early pre-tangle pathology (representative images are displayed in Figs. 6 and 7). TNT1 and TNT2 both labeled early tau pathology in all disease stages, but the TNT1 and TNT2 reactivity was lost in several late-stage NFTs, many of which lacked nuclei suggesting they were ghost tangles (Figs. 6 and 7). In the Braak I–II cases, TNT1 and TNT2 presented a diffuse, granular staining pattern that is characteristic of group 1 neurons (Figs. 6A and 7A). These inclusions were ThR negative, indicating a lack of mature fibrillary tau aggregates containing β-sheet structures. Neurons presenting the granular tau staining pattern were still present in Braak III–IV cases but more compact pathology also appeared (Figs. 6B and 7B) that was positive for ThR (i.e., group 2 and 3 cells). In Braak V–VI cases, a third distinct population of cells appeared that were ThR positive but negative for

TNT1 or TNT2 (likely late group 3 cells or ghost tangles; Figs. 6C and 7C). We also performed IF staining in hippocampal sections with PHF1 and ThR (Supp. Fig. 4). Like the TNT antibodies, the PHF1 phosphoepitope was present in early pre-tangle group 1 cells that were ThR negative in all Braak stages and also present in ThR-positive group 2 and 3 cells in later Braak stages (Supp. Fig. 4). However, ThR-positive cells that were PHF1 negative were infrequent and several apparent ghost tangles remained PHF1-reactive (Supp. Fig. 4I–L).

Next, we performed multi-label IF with TNT1 or TNT2, ThR, DAPI, and the Alz50 antibody, an established tau conformation-specific antibody that appears in early pre-tangle neurons, to further confirm that TNT1 and TNT2 labeled early tau pathology (Carmel et al., 1996; Hyman et al., 1988; Jicha et al., 1997). Both TNT1 and TNT2 showed extensive colocalization with Alz50 in all stages of the disease (Supp. Figs. 5 and 6). As above, there were three distinct populations of cells found through the Braak stages: TNT1+/TNT2+, Alz50+ and ThR−(group 1 cells), TNT1+/TNT2+, Alz50+, and ThR+ (group 2 and 3 cells), or TNT1−/TNT2−, Alz50−, and ThR+ (late group 3 or ghost tangles).

5. Discussion

Tau dysfunction is likely a key mediator of neurodegeneration in Alzheimer's disease and other tauopathies; however, the mechanisms of tau toxicity are not entirely clear. Historically, the amino terminus of tau has largely been ignored, with most of the focus placed on the microtubule-binding domains due to their involvement in microtubule binding and β-sheet formation in tau aggregates. Previous work established that the N-terminus is important for other biological functions of tau and tau's role in disease pathogenesis (Brandt et al., 1995; Horowitz et al., 2006). More recently, our group established that the first 18 amino acids of tau comprise a biologically active motif, called the phosphatase-activating domain or PAD, and exposure of this motif is both necessary and sufficient to disrupt anterograde fast axonal transport in squid axoplasm (Kanaan et al., 2011). PAD exposure initiated a PP1-GSK3β signaling cascade that resulted in phosphorylation of kinesin light chain and dissociation of bound cargoes (Kanaan et al., 2011). These studies highlight important characteristics of the amino terminus and suggest that this region of the molecule is critical in understanding tau-mediated toxicity. Thus, we have recently shifted our focus to the PAD motif and here we utilized several N-terminal tau antibodies to examine details about PAD exposure in the context of human disease.

5.1. Refining N-terminal tau antibody epitopes and characterizing the novel TNT2 antibody

Performing a detailed characterization of the epitopes of TNT1, TNT2, Tau12, and Tau13 was the first step in establishing the differences between these antibodies and determining their abilities to identify PAD exposure. A peptide of amino acids 2–18 in tau was used to raise TNT1 and TNT2, but through the use of a scanning alanine mutation approach, we refined the epitope of both TNT antibodies to amino acids 7–12. Mutations at the edges of the TNT1 and TNT2 epitopes partially disrupted antibody binding, and overall, these antibodies were not as effective in denaturing western blots compared to Tau12 and Tau13, further supporting that optimal TNT1 and TNT2 reactivity is dependent on native

conformation. Finally, we demonstrated that all of these N-terminal antibodies were specific for tau (no reactivity in tau knockout mouse samples) and both TNT antibodies cross-react with mouse and rat tau, despite two amino acid differences (i.e., E9D and V10T) between human and rodent tau.

Using larger deletion constructs, the Tau12 epitope was previously mapped to amino acids 2–23 (Horowitz et al., 2004) and the Tau13 epitope to within amino acids 9–18 (Garcia-Sierra et al., 2003; Ghoshal et al., 2002). The alanine mutation approach showed that Tau12 and Tau13 have discontinuous epitopes composed of amino acids 8–9 and 13–21, but some differences were noted. For example, changing amino acids 8 and 9 completely disrupted reactivity of Tau12 but not Tau13. In fact, the reactivity of the Tau13 antibody was not completely abolished with any of these discrete modifications, likely due to the very high affinity of this antibody (highest of those tested here). However, coupling these data with previous deletion construct data (Garcia-Sierra et al., 2003; Ghoshal et al., 2002), as well as a lack of reactivity to the Δ2–18 tau deletion construct shown here, suggests that the important amino acids in the Tau13 epitope are 8–9 and 13–21. Both Tau12 and Tau13 are sensitive and, as previously reported (Petry et al., 2014), human-specific antibodies (i.e., lack reactivity with all rodent tau), which is consistent with the absence of human amino acids 19–28 in rodent tau and further supports a distinction between the epitope of these and the TNT antibodies.

5.2. Differential reactivity among N-terminal antibodies and identification of PAD exposure

Previously, we have shown that TNT1 is a marker of PAD exposure and that this event occurs early in the progression of Alzheimer's disease. Establishing whether this was true for all N-terminal antibodies was important for understanding more about PAD exposure in Alzheimer's disease. We significantly extend these findings with TNT1 and show that TNT2 behaves similarly as a marker of PAD exposure. In contrast, other N-terminal antibodies, with slightly different epitopes, do not function as pathological, PAD exposure-specific markers and recognize all forms of tau similarly. Despite its reputation as an "intrinsically disordered" protein, tau is known to exist in a global conformation and contains regions of important secondary structure (Jeganathan et al., 2006; Mukrasch et al., 2009). PAD exposure is heavily dependent upon tau conformation (Jeganathan et al., 2008; Kanaan et al., 2011). In native-state biochemical assays, both TNT1 and TNT2 show remarkable selectivity and strong reactivity with pathological tau (e.g., aggregated recombinant protein and tau from Alzheimer's disease brains), but not normal tau (e.g., recombinant monomers or tau from control brains). Importantly, the R1 antibody used for detection in these assays is a polyclonal antibody with epitopes throughout the entire tau protein (Berry et al., 2004) suggesting that these N-terminal antibodies will not negatively affect R1 binding. Indeed, deletion of amino acids 2–18 did not eliminate R1 reactivity in western blots, and pre-labeling tau with N-terminal antibodies does not appreciably affect R1 binding in indirect ELISAs (unpublished observation). The dependence of conformation was apparent as TNT1 and TNT2 lose their selectivity for pathological tau in denaturing SDS-PAGE western blots. Additionally, these antibodies demonstrated very high affinity for monomeric recombinant tau in indirect ELISAs suggesting the protein undergoes denaturation upon binding to the polystyrene plate, which has been noted with other proteins (Hollander and Katchalski-

Katzir, 1986; Shields et al., 1991). TNT2 appears to be more sensitive to these conformational changes as evidenced by its greater reactivity in the non-denaturing assays as well as its stronger labeling of tau pathology in human tissue.

The uniqueness of the TNT1 and TNT2 reactivity profile is further highlighted by the lack of such selectivity for pathological tau with Tau12 and Tau13. These differences in antibody reactivity are directly related to slight differences in their respective epitopes within the extreme N-terminus of tau. This suggests that reactivity could depend on a secondary structure within this region that is typically obscured or not present in monomeric tau but is exposed or stabilized in pathological tau. Secondary structure in this region has not been experimentally demonstrated but an α-helix is predicted to exist from amino acids 7–12 (Gamblin, 2005). Larger conformational changes could leave this epitope exposed or affect stability of the α-helix, thereby greatly enhancing antibody reactivity. Interestingly, TNT1 and TNT2, in particular, are less effective in the denaturing conditions of a western blot, indicating that some protein structure may enhance reactivity. In contrast, inclusion of amino acids 13–21 in the epitope of Tau12 and Tau13 appears to drive the lack of distinction between normal and pathological tau, suggesting that these downstream amino acids are accessible in all forms of tau.

5.3. Timing of PAD exposure in human disease

The N-terminal antibodies in this study were also used to characterize PAD exposure and tau deposition in human post-mortem brain sections. Reactive neurons were categorized into previously established phenotypes based on the stage of tau inclusion formation within the cells (Bancher et al., 1989, 1991; Braak et al., 1994). Previous observations showing that TNT1 appeared to precede AT8 (Kanaan et al., 2011), a phosphoepitope that appears early in pathology formation, suggested that PAD exposure occurred very early in pre-tangle neurons (Braak et al., 1994; Garcia-Sierra et al., 2000; Kanaan et al., 2012; Luna-Munoz et al., 2007). Here, we found that TNT1 and TNT2 appear in Braak I–II stages and do not colocalize with ThR in the diffuse, granular pre-tangle pathology conclusively demonstrating that PAD exposure is an early event. As noted previously, ThR fluorescence was largely absent until the Braak III–IV cases when more compact NFT tau inclusions form (Mena et al., 1995). Importantly, we show that group 1 and 2 neurons, primarily labeled by TNT1 and TNT2 in the early Braak stages, are present through the latest Braak stages in roughly the same numbers. This finding highlights the asynchronous and continual nature of PAD exposure and tau inclusion formation during the progression of Alzheimer’s disease. Moreover, our data suggest that early PAD exposure is one of the mechanisms behind soluble and oligomeric tau toxicity (Kanaan et al., 2011, 2012; Patterson et al., 2011a, 2011b).

The TNT antibodies also label classic NFT-containing group 3 neurons in later Braak stages, which colocalize with ThR. Apparent ThR-positive ghost tangles (i.e., without nuclei (Braak et al., 1994)) are no longer labeled by TNT1 or TNT2, which confirms that PAD exposure is lost in the latest stages of NFT evolution. The disappearance of TNT labeling is not unexpected as the loss of the extreme N-terminus in compact NFTs and ghost tangles were previously reported in several studies (Bondareff et al., 1994; Dickson et al., 1992; Endoh et

al., 1993; Horowitz et al., 2004). Proteolysis with caspase-6, a known mediator of tau degradation, particularly at the D13 site, may cause the loss of TNT antibody reactivity as it does Tau12 reactivity (Guo et al., 2004; Horowitz et al., 2004). N-terminal cleavage in mature NFTs could have important implications for tau toxicity in Alzheimer's disease as degradation would include a loss of PAD. This could reduce aberrant PAD-induced PP1-GSK3β signaling and axonal transport defects, potentially leading to NFTs that are less toxic than oligomers and other pre-tangle forms of tau pathology. Loss of TNT reactivity also explains the differences when compared to PHF1, a well-known phosphoepitope in tau (pS396/pS404) (Greenberg et al., 1992; Otvos et al., 1994), known to persist in late-stage NFTs (Augustinack et al., 2002). The staining patterns were similar until Braak stages V–VI when PHF1 labeled many more group 3 and 4 cells (e.g. ghost tangles). These differences support the notion that modifications and epitopes are differentially changed during the evolution of tau pathology.

Tau12 and Tau13 showed similar patterns of reactivity throughout the different Braak stages, but these antibodies also robustly labeled parenchymal tau. This staining pattern is consistent with labeling normal endogenous tau proteins (Papasozomenos and Binder, 1987) and is not surprising considering their inability to differentiate between normal and misfolded tau in biochemical assays. In contrast, TNT1 and, to an even greater degree, TNT2 displayed a very strong preference for pathological tau and little to no parenchymal tau staining. This is one of the most important distinctions between the TNT antibodies and the other N-terminal antibodies studied here. Again, this demonstrates that the PAD exposure phenotype is specific to pathological forms of tau and is dependent on effects within the TNT1 and TNT2 epitopes (i.e. amino acids 7–12) but not the Tau12 and Tau13 epitopes that are just slightly downstream.

Finally, we performed co-immunofluorescence stains of TNT1 or TNT2 with Alz50 to determine how these N-terminal antibodies compare to an established marker of early pathological conformational changes (Carmel et al., 1996; Hyman et al., 1988). Extensive colocalization existed between the TNT antibodies and Alz50 in all Braak stages and all cellular phenotypes (i.e., groups 1–3 cells). It is noteworthy that the epitopes of the TNT and Alz50 antibodies overlap and that the EC_{50} value of Alz50 in an indirect ELISA with recombinant tau (24.50 ng/ml, data not shown) is quite close to that of TNT1 and TNT2 in molarity (Alz50 has a higher molecular weight as an IgM while TNT1 and TNT2 are IgG1 antibodies). These data suggest that there is direct competition for binding sites and this could lead to underestimations of each form of tau with these dual label stains. Despite this limitation, the high level of colocalization suggests the conformations that give rise to PAD exposure and the discontinuous epitope of Alz50 occur simultaneously in tau pathology. Importantly, the involvement of additional regions of tau protein for reactivity of Alz50 (Carmel et al., 1996) and MC1 (Jicha et al., 1997) mitigate their usefulness as direct markers of PAD exposure.

6. Conclusions

There has long been a link between tau misfolding and tau pathology. Recent evidence shows that disease-related modifications of tau cause abnormal exposure of PAD leading to

axonal dysfunction and highlighting the importance of tau's amino terminus. Here, through the use of N-terminal tau antibodies, we examine these changes as tau progresses from normal to a pathological form. We demonstrate that TNT1 and TNT2 are strong markers for PAD exposure in pathological forms of tau while other N-terminal antibodies like Tau12 and Tau13 are unable to differentiate between the two forms. The uniqueness of the TNT antibodies and their interaction with the pathological changes associated with these conformational changes are due to their specific epitopes (i.e. amino acids 7–12), as it is not replicated with N-terminal antibodies that bind to locations slightly downstream. Due to the conformation-dependent specificity of TNT1 and TNT2, we provide strong evidence that PAD exposure occurs early during pathological tau deposition in human brains but the epitope is lost in late neurofibrillary tangles or ghost tangles. Given the previously demonstrated link between PAD exposure and toxic disruptions in anterograde fast axonal transport, this provides a potential explanation for toxicity associated with earlier forms of pathological tau but not mature neurofibrillary tangles. The data support changes in the N-terminus as a key identifier of dysfunctional tau, a finding that may have important implications for tau toxicity and the pathogenesis of Alzheimer's disease.

Supplementary Material

Refer to Web version on PubMed Central for supplementary material.

Acknowledgments

Funding

This study was funded by NIH/NIA R01 AG044372 (NMK), NIH/NINDS R01 NS082730 (NMK), BrightFocus Foundation (A2013364S, NMK), and Secchia Family Foundation Research Fund (NMK).

We gratefully acknowledge the late Lester "Skip" Binder for deepening our understanding of the tau protein and his long-lasting impact on the field through his numerous contributions (including some of the antibodies used here), Tessa Grabinski for her technical help with purifying tau antibodies, and Peter Davies for the Alz50 antibody. We would like to acknowledge the Neuropathology Core in the Alzheimer Disease Core Center at Northwestern University, Chicago, Illinois, for providing the human brain tissue.

Abbreviations

NFT	Neurofibrillary tangles
PAD	Phosphatase-activating domain
ThR	Thiazine red
ELISA	Enzyme-linked immunosorbent assay
TNT	Tau N-terminal antibody
DTT	dithiothreitol
BSA	bovine serum albumin
TMB	3,3′,5,5′-tetramethylbenzidine
TBS	tris buffered saline

AD	Alzheimer's disease
DAB	3,3′-diaminobenzidine
IHC	immunohistochemistry
PP1	protein phosphatase 1
GSK	glycogen synthase kinase

References

Augustinack JC, et al. Specific tau phosphorylation sites correlate with severity of neuronal cytopathology in Alzheimer's disease. Acta Neuropathol (Berl). 2002; 103:26–35. [PubMed: 11837744]

Bancher C, et al. Accumulation of abnormally phosphorylated tau precedes the formation of neurofibrillary tangles in Alzheimer's disease. Brain Res. 1989; 477:90–99. [PubMed: 2495152]

Bancher C, et al. Abnormal phosphorylation of tau precedes ubiquitination in neurofibrillary pathology of Alzheimer disease. Brain Res. 1991; 539:11–18. [PubMed: 1849776]

Berry RW, et al. Tau epitope display in progressive supranuclear palsy and corticobasal degeneration. J Neurocytol. 2004; 33:287–295. [PubMed: 15475684]

Bobinski M, et al. Relationships between regional neuronal loss and neurofibrillary changes in the hippocampal formation and duration and severity of Alzheimer disease. J Neuropathol Exp Neurol. 1997; 56:414–420. [PubMed: 9100672]

Bondareff W, et al. Immunohistochemical staging of neurofibrillary degeneration in Alzheimer's disease. J Neuropathol Exp Neurol. 1994; 53:158–164. [PubMed: 7509849]

Braak H, Braak E. Neuropathological stageing of Alzheimer-related changes. Acta Neuropathol. 1991; 82:239–259. [PubMed: 1759558]

Braak E, et al. A sequence of cytoskeleton changes related to the formation of neurofibrillary tangles and neuropil threads. Acta Neuropathol (Berl). 1994; 87:554–567. [PubMed: 7522386]

Brandt R, et al. Interaction of tau with the neural plasma membrane mediated by tau's amino-terminal projection domain. J Cell Biol. 1995; 131:1327–1340. [PubMed: 8522593]

Bussiere T, et al. Stereologic analysis of neurofibrillary tangle formation in prefrontal cortex area 9 in aging and Alzheimer's disease. Neuroscience. 2003; 117:577–592. [PubMed: 12617964]

Carmel G, et al. The structural basis of monoclonal antibody Alz50's selectivity for Alzheimer's disease pathology. J Biol Chem. 1996; 271:32789–32795. [PubMed: 8955115]

Dickson DW, et al. Immunocytochemistry of neurofibrillary tangles with antibodies to subregions of tau protein: identification of hidden and cleaved tau epitopes and a new phosphorylation site. Acta Neuropathol. 1992; 84:596–605. [PubMed: 1281953]

Endoh R, et al. Lack of the carboxyl terminal sequence of tau in ghost tangles of Alzheimer's disease. Brain Res. 1993; 601:164–172. [PubMed: 8431763]

Gamblin TC. Potential structure/function relationships of predicted secondary structural elements of tau. Biochim Biophys Acta. 2005; 1739:140–149. [PubMed: 15615633]

Gamblin TC, et al. In vitro polymerization of tau protein monitored by laser light scattering: method and application to the study of FTDP-17 mutants. Biochemistry. 2000; 39:6136–6144. [PubMed: 10821687]

Garcia-Sierra F, et al. The extent of neurofibrillary pathology in perforant pathway neurons is the key determinant of dementia in the very old. Acta Neuropathol (Berl). 2000; 100:29–35. [PubMed: 10912917]

Garcia-Sierra F, et al. Conformational changes and truncation of tau protein during tangle evolution in Alzheimer's disease. J Alzheimers Dis. 2003; 5:65–77. [PubMed: 12719624]

Ghoshal N, et al. Tau conformational changes correspond to impairments of episodic memory in mild cognitive impairment and Alzheimer's disease. Exp Neurol. 2002; 177:475–493. [PubMed: 12429193]

Goedert M, et al. Monoclonal antibody AT8 recognises tau protein phosphorylated at both serine 202 and threonine 205. Neurosci Lett. 1995; 189:167–169. [PubMed: 7624036]

Gomez-Isla T, et al. Neuronal loss correlates with but exceeds neurofibrillary tangles in Alzheimer's disease. Ann Neurol. 1997; 41:17–24. [PubMed: 9005861]

Greenberg SG, et al. Hydrofluoric acid-treated tau PHF proteins display the same biochemical properties as normal tau. J Biol Chem. 1992; 267:564–569. [PubMed: 1370450]

Guo H, et al. Active caspase-6 and caspase-6-cleaved tau in neuropil threads, neuritic plaques, and neurofibrillary tangles of Alzheimer's disease. Am J Pathol. 2004; 165:523–531. [PubMed: 15277226]

Hollander Z, Katchalski-Katzir E. Use of monoclonal antibodies to detect conformational alterations in lactate dehydrogenase isoenzyme 5 on heat denaturation and on adsorption to polystyrene plates. Mol Immunol. 1986; 23:927–933. [PubMed: 3785230]

Horowitz PM, et al. Early N-terminal changes and caspase-6 cleavage of tau in Alzheimer's disease. J Neurosci. 2004; 24:7895–7902. [PubMed: 15356202]

Horowitz PM, et al. N-terminal fragments of tau inhibit full-length tau polymerization in vitro. Biochemistry. 2006; 45:12859–12866. [PubMed: 17042504]

Hyman BT, et al. Alz-50 antibody recognizes Alzheimer-related neuronal changes. Ann Neurol. 1988; 23:371–379. [PubMed: 3382173]

Jeganathan S, et al. Global hairpin folding of tau in solution. Biochemistry. 2006; 45:2283–2293. [PubMed: 16475817]

Jeganathan S, et al. Proline-directed pseudo-phosphorylation at AT8 and PHF1 epitopes induces a compaction of the paperclip folding of tau and generates a pathological (MC-1) conformation. J Biol Chem. 2008; 283:32066–32076. [PubMed: 18725412]

Jicha GA, et al. Alz-50 and MC-1, a new monoclonal antibody raised to paired helical filaments, recognize conformational epitopes on recombinant tau. J Neurosci Res. 1997; 48:128–132. [PubMed: 9130141]

Jicha GA, et al. Sequence requirements for formation of conformational variants of tau similar to those found in Alzheimer's disease. J Neurosci Res. 1999; 55:713–723. [PubMed: 10220112]

Kanaan NM, et al. Pathogenic forms of tau inhibit kinesin-dependent axonal transport through a mechanism involving activation of axonal phosphotransferases. J Neurosci. 2011; 31:9858–9868. [PubMed: 21734277]

Kanaan NM, et al. Phosphorylation in the amino terminus of tau prevents inhibition of anterograde axonal transport. Neurobiol Aging. 2012; 33(826):e15–e30. [PubMed: 21794954]

Kanaan NM, et al. Characterization of early pathological tau conformations and phosphorylation in chronic traumatic encephalopathy. J Neuropathol Exp Neurol. 2015

Kapuscinski J. DAPI: a DNA-specific fluorescent probe. Biotech Histochem. 1995; 70:220–233. [PubMed: 8580206]

LaPointe NE, et al. The amino terminus of tau inhibits kinesin-dependent axonal transport: implications for filament toxicity. J Neurosci Res. 2009; 87:440–451. [PubMed: 18798283]

Luna-Munoz J, et al. Earliest stages of tau conformational changes are related to the appearance of a sequence of specific phospho-dependent tau epitopes in Alzheimer's disease. J Alzheimers Dis. 2007; 12:365–375. [PubMed: 18198423]

Mena R, et al. Monitoring pathological assembly of tau and beta-amyloid proteins in Alzheimer's disease. Acta Neuropathol. 1995; 89:50–56. [PubMed: 7709731]

Mercken M, et al. Monoclonal antibodies with selective specificity for Alzheimer tau are directed against phosphatase-sensitive epitopes. Acta Neuropathol. 1992; 84:265–272. [PubMed: 1384266]

Morsch R, et al. Neurons may live for decades with neurofibrillary tangles. J Neuropathol Exp Neurol. 1999; 58:188–197. [PubMed: 10029101]

Mukrasch MD, et al. Structural polymorphism of 441-residue tau at single residue resolution. PLoS Biol. 2009; 7:e34. [PubMed: 19226187]

Otvos L Jr, et al. Monoclonal antibody PHF-1 recognizes tau protein phosphorylated at serine residues 396 and 404. J Neurosci Res. 1994; 39:669–673. [PubMed: 7534834]

Papasozomenos SC, Binder LI. Phosphorylation determines two distinct species of tau in the central nervous system. Cell Motil Cytoskeleton. 1987; 8:210–226. [PubMed: 2446784]

Patterson KR, et al. Characterization of prefibrillar Tau oligomers in vitro and in Alzheimer disease. J Biol Chem. 2011a; 286:23063–23076. [PubMed: 21550980]

Patterson KR, et al. Heat shock protein 70 prevents both tau aggregation and the inhibitory effects of preexisting tau aggregates on fast axonal transport. Biochemistry. 2011b; 50:10300–10310. [PubMed: 22039833]

Petry FR, et al. Specificity of anti-tau antibodies when analyzing mice models of Alzheimer's disease: problems and solutions. PLoS One. 2014; 9:e94251. [PubMed: 24788298]

Santacruz K, et al. Tau suppression in a neurodegenerative mouse model improves memory function. Science. 2005; 309:476–481. [PubMed: 16020737]

Shields MJ, et al. An appraisal of polystyrene-(ELISA) and nitrocellulose-based (ELIFA) enzyme immunoassay systems using monoclonal antibodies reactive toward antigenically distinct forms of human C-reactive protein. J Immunol Methods. 1991; 141:253–261. [PubMed: 1880430]

Spires-Jones TL, et al. In vivo imaging reveals dissociation between caspase activation and acute neuronal death in tangle-bearing neurons. J Neurosci. 2008; 28:862–867. [PubMed: 18216194]

Wittmann CW, et al. Tauopathy in drosophila: neurodegeneration without neurofibrillary tangles. Science. 2001; 293:711–714. [PubMed: 11408621]

Yoshiyama Y, et al. Synapse loss and microglial activation precede tangles in a P301S tauopathy mouse model. Neuron. 2007; 53:337–351. [PubMed: 17270732]

Appendix A. Supplementary data

Supplementary data to this article can be found online at http://dx.doi.org/10.1016/j.nbd.2016.05.016.

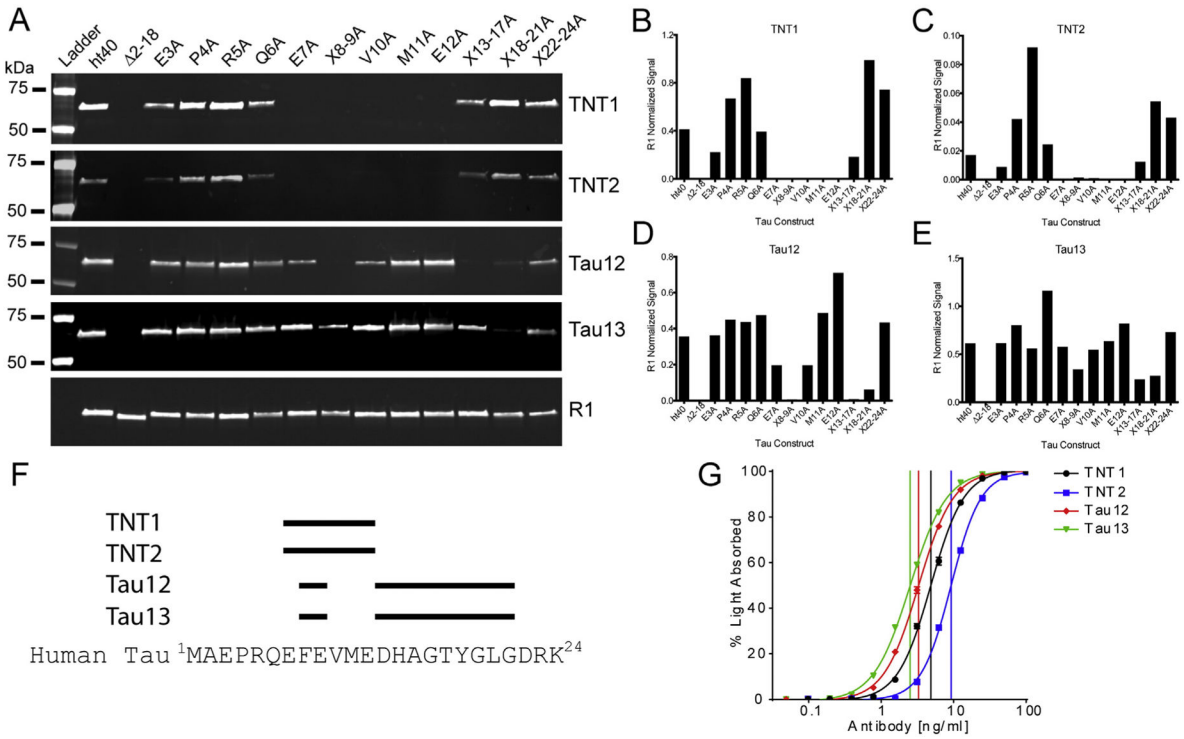

Fig. 1. Antibodies recognize similar but distinct epitopes with high affinity

(*A*–*E*) The epitopes were mapped using scanning alanine mutant tau proteins in western blots. (*A*) TNT1 reactivity was eliminated upon mutating amino acids 7–12. Similarly, TNT2 reactivity was disrupted with mutation of amino acids 7–12, and TNT2 displayed less reactivity in general compared to the other antibodies in western blotting. The Tau12 epitope (previously mapped to 2–23 (Horowitz et al., 2004)) was discontinuous as mutating amino acids 8–9 and 13–21 had a strong impact on reactivity. Tau13 is a very high-affinity antibody (previously mapped to 9–18 (Garcia-Sierra et al., 2003)), and similar to Tau12, reactivity for Tau13 was affected by mutating amino acids 8–9, and 13–21. Notably, none of the alanine mutant constructs completely eliminated reactivity, but deletion of amino acids 2–18 completely eliminated reactivity as before (Garcia-Sierra et al., 2003). The R1 tau antibody, a rabbit polyclonal total tau antibody with epitopes throughout the protein (i.e., unaffected by mutant protein changes), was used to identify total levels of all protein constructs. (*B*–*E*) Signal intensity was quantified for (*B*) TNT1, (*C*) TNT2, (*D*) Tau12, and (*E*) Tau13 and normalized to R1 signal to confirm elimination/reduction in reactivity with each recombinant tau protein. (*F*) A schematic representing the specific epitopes for each antibody (TNT1 and TNT2: 7–12; Tau12 and Tau13: 8–9, 13–21) and showing sequence alignments between the first 24 amino acids of human tau. (*G*) N-terminal antibody-binding affinities for full-length recombinant tau in indirect ELISAs. The antibodies (ranging from 48.8 pg/ml to 100 ng/ml) were incubated with recombinant tau (100 ng/well) bound to a titer ELISA plate. The data were fit to a sigmoidal dose–response curve and EC_{50} values were determined (vertical lines), indicating the antibody concentration at which half of the maximum signal is obtained. TNT1 (black circles) EC_{50} = 4.86 ng/ml, TNT2 (blue squares)

EC_{50} = 9.21 ng/ml, Tau12 (red diamonds) EC_{50} = 3.27 ng/ml, Tau13 (green triangles) EC_{50} = 2.51 ng/ml.

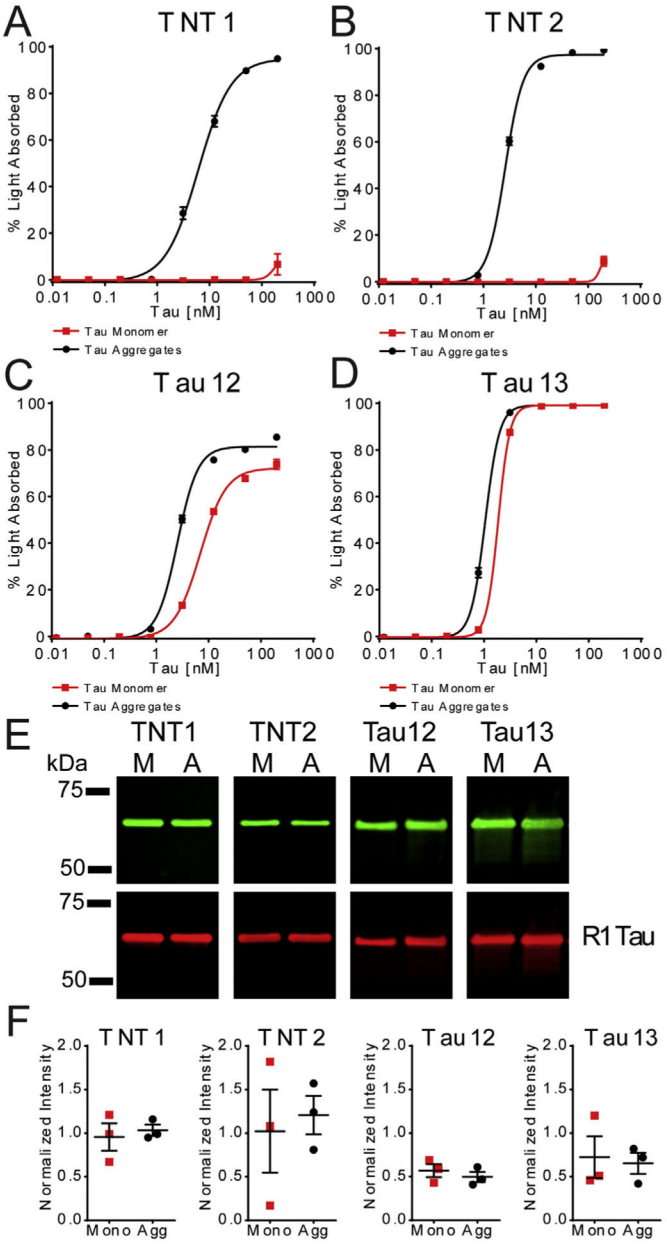

Fig. 2. TNT1 and TNT2 binding is selective for aggregated tau and is conformation dependent

(*A*–*D*). The binding affinity of (*A*) TNT1, (*B*) TNT2, (*C*) Tau12, and (*D*) Tau13 for monomeric and aggregated recombinant tau samples (ranging from 12.2 pM to 200 nM) were measured using sandwich ELISAs ($n = 3$; mean ± SEM). (*A*) TNT1 showed reactivity with aggregated tau (black circles) starting at 3.125 nM (EC_{50} = 6.0 nM) but did not detect monomeric tau (red squares) until it reached 200 nM (EC_{50} = undetermined). (*B*) Similarly, TNT2 robustly reacted with aggregated tau starting at 0.781 nM (TNT2: EC_{50} = 2.6 nM) but did not detect monomeric tau until it reached 200 nM (EC_{50} = undetermined). (*C*) Tau12 displayed a slight preference for aggregated tau (EC_{50} = 6.9 nM) over monomeric tau (EC_{50} = 2.5 nM). (*D*) Tau13 recognized monomeric (EC_{50} = 1.9 nM) and aggregated (EC_{50} = 1.1

nM) tau similarly at all concentrations. (*E*) The same monomer and aggregated tau samples were denatured and run on SDS-PAGE/western blots to determine whether the aggregated tau-selective reactivity was conformation-dependent. Representative blots with TNT1, TNT2, Tau12, and Tau13 demonstrating equal reactivity to the denatured monomeric and aggregated samples (top). Equivalent amounts of tau were confirmed with R1, a pan-tau antibody (bottom). (*F*) The signal intensities associated with each antibody's reactivity to monomeric (red squares) and aggregated (black circles) tau samples were quantified and normalized to the R1 values. This quantitation showed equal reactivity in western blots with TNT1: $p = 0.593$, $t(2) = 0.630$; TNT2: $p = 0.550$, $t(2) = 0.713$; Tau12: $p = 0.368$, $t(2) = 1.153$; Tau13: $p = 0.742$, $t(2) = 0.378$ (compared with paired *t*-tests).

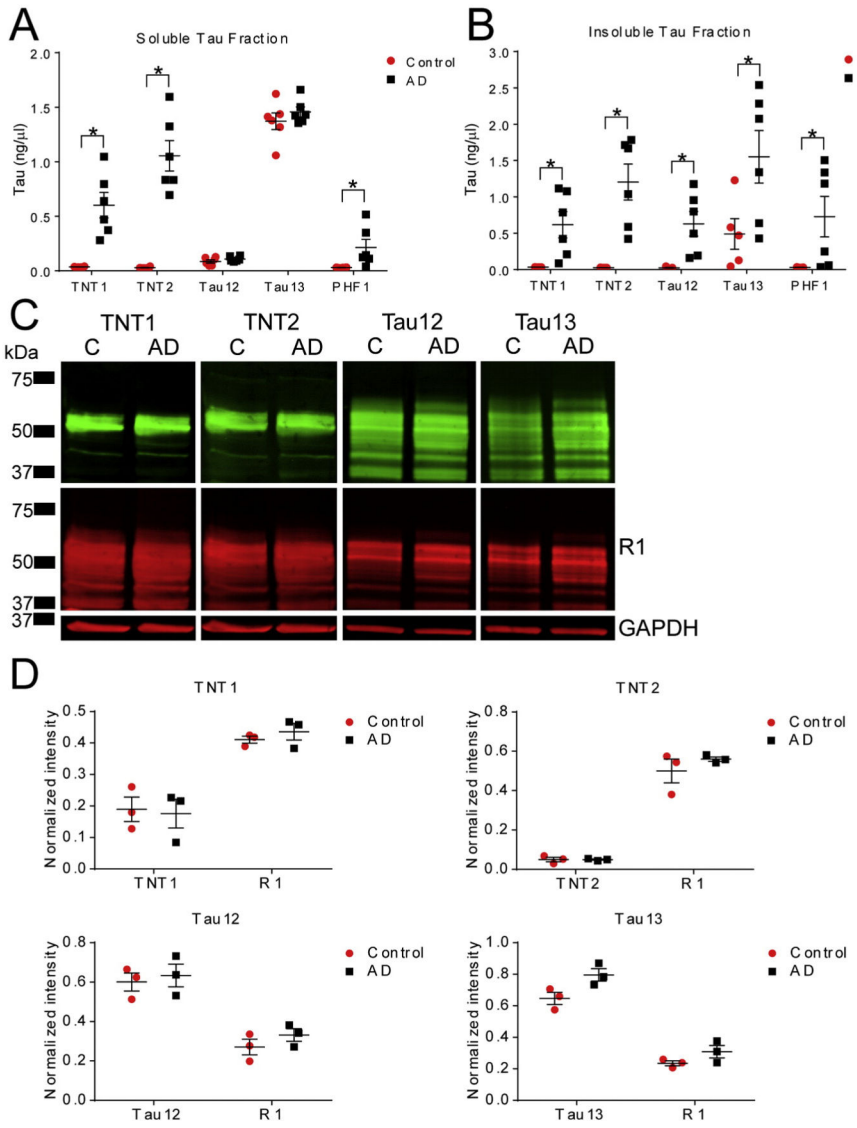

Fig. 3. TNT1 and TNT2 recognize pathological but not normal tau dependent upon conformation

TNT1 and TNT2 display conformation-dependent recognition of PAD-exposed tau in Alzheimer's disease, which is not present in non-demented controls. (*A*) Soluble protein fractions from human frontal cortex lysates of control and AD brains were used in sandwich ELISAs using TNT1, TNT2, Tau12, Tau13, or PHF1 as the capture antibody. TNT1, TNT2, and PHF1 all detected significantly more tau in AD lysates (black squares) than in control lysates (red circles) ($n = 6$; mean ± SEM; $^{*}p < 0.05$, unpaired *t*-test, TNT1: $t(10) = 4.843$, $p = 0.0007$; TNT2: $t(10) = 7.303$; $p < 0.0001$; Tau12: $t(10) = 1.228$; $p = 0.2475$; Tau13: $t(10) = 0.9758$; $p = 0.3522$; PHF1: ($t(10) = 2.504$; $p = 0.0312$)). (*B*) Sandwich ELISAs were also carried out with sarkosyl-insoluble protein fractions from human frontal cortex lysates of control and AD brains. Significantly more tau was detected in the sarkosyl-insoluble protein fractions from AD lysates than the control lysates with all antibodies ($n = 5$ for control and $n = 6$ AD; mean ± SEM; $^{*}p < 0.05$, unpaired *t*-test, TNT1: ($t(9) = 2.923$; $p = 0.0169$), TNT2: ($t(9) = 4.301$; $p = 0.002$), Tau12: ($t(9) = 3.228$; $p = 0.0103$), Tau13: ($t(9) = 2.398$; $p = 0.04$)

and PHF1: ($t(9) = 2.264$; $p = 0.0499$)). (*C*) The soluble fractions for control and AD brains were run under denaturing conditions in western blots. Samples were loaded at 60 μg total protein/lane for TNT1 and TNT2 and 20 μg total protein/lane for Tau12 and Tau13. GAPDH was used as a loading control to confirm equal loading and R1, a pan-tau antibody, was used to determine the total amounts of tau in the samples. Notably, TNT1 and TNT2 did not work as well as Tau12 or Tau13 in western blot assays. (*D*) Tau signal intensities from the control and AD western blots were quantified and normalized to the GAPDH signal. All antibodies detected similar levels of tau in the control samples (red circles) compared to the AD samples (black squares) under denaturing conditions (mean ± SEM, $p > 0.05$ for all comparisons in unpaired *t*-tests, TNT1: $t(4) = 0.234$, $p = 0.827$; TNT2: $t(4) = 0.029$, $p = 0.978$; Tau12: $t(4) = 0.451$, $p = 0.675$; Tau13: $t(4) = 2.699$, $p = 0.055$). Detection with the pan-tau R1 antibody confirmed that similar amounts of tau were present in the control and AD samples (mean ± SEM, $p > 0.05$ for all comparisons in unpaired *t*-tests, $t(4) = 0.881$, $p = 0.428$ (TNT1 blot); $t(4) = 0.984$, $p = 0.381$ (TNT2 blot); $t(4) = 1.198$, $p = 0.297$ (Tau12 blot); $t(4) = 1.727$, $p = 0.159$ (Tau13 blot)).

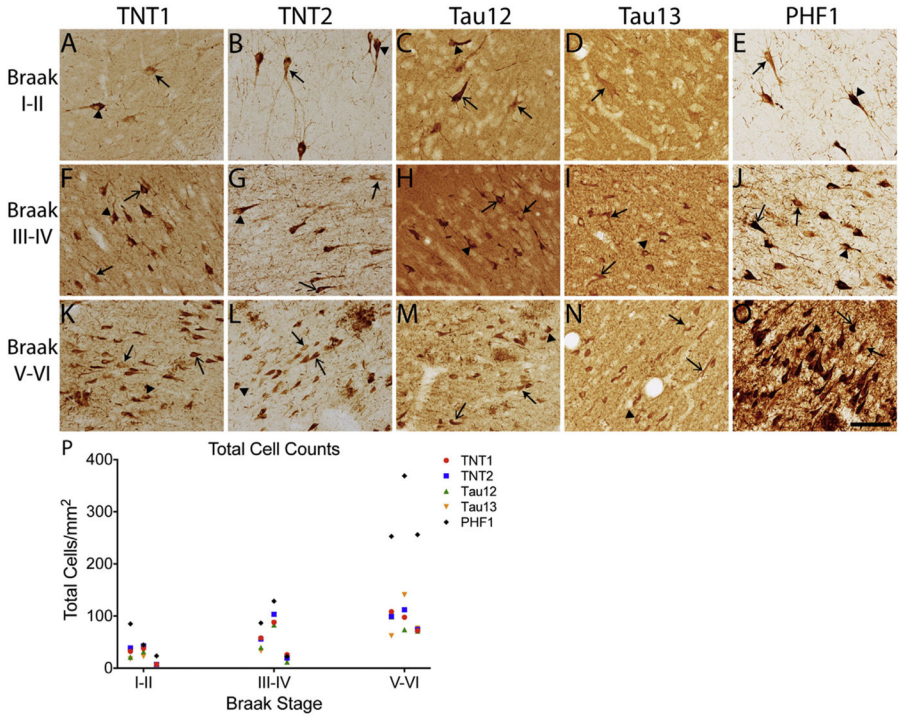

Fig. 4. N-terminal antibodies label early tau pathology in the hippocampus and the extent of pathology increases with advancing Braak stage

(*A*) TNT1, (*B*) TNT2, (*C*) Tau12, (*D*) Tau13, and (*E*) PHF1 labeled diffuse, granular pre-tangle neurons in hippocampal neurons of Braak stage I–II cases. There was a notable difference in the extent of parenchymal tau labeled by each of the antibodies. TNT1, TNT2, and PHF1 produced little to no parenchymal tau signal. In contrast, both Tau12 and Tau13 robustly labeled parenchymal tau (i.e., non-pathological tau). (*F–J*) In Braak stage III–IV cases, (*F*) TNT1, (*G*) TNT2, (*H*) Tau12, (*I*) Tau13, and (*J*) PHF1 detected increased pathology and more compact tau inclusions characteristic of group 2 and 3 neurons. Tau12 (*H*) and Tau13 (*I*) continued to strongly label parenchymal tau, and neuritic threads were not as evident. (*K—O*) The extent of (*K*) TNT1-, (*L*) TNT2-, (*M*) Tau12-, and (N) Tau13-positive pathology continued to increase and early pre-tangle neurons were still present in late-stage cases. (*M*) Tau12 and (*N*) Tau13 labeled early tau pathology and parenchymal tau but at lower levels than in the earlier cases. (*O*) PHF1 displayed intense reactivity to the tau pathology with the vast majority representing classic NFTs, as well as robust thread labeling. Examples of neurons with diffuse, granular pre-tangle pathology (i.e., group 1) are identified with closed arrows, intermediate neurons containing a combination of granular and compact inclusions (i.e., group 2) are identified with closed arrowheads, and classic, compact neurofibrillary tangles (i.e., group 3) are identified with open arrows. Scale bar represents 100 μm. (*P*) The cell density of all neurons labeled with each N-terminal antibody (TNT1, red circles; TNT2, blue squares; Tau12, green triangles; Tau13, orange triangles; PHF1, black diamonds) showed a strong, significant positive correlation with increasing Braak stage (TNT1: $r = 0.791$, $p = 0.021$; TNT2: $r = 0.738$, $p = 0.037$; Tau12: $r = 0.738$, $p = 0.037$; Tau13: $r = 0.738$, $p = 0.037$; PHF1: $r = 0.791$, $p = 0.021$).

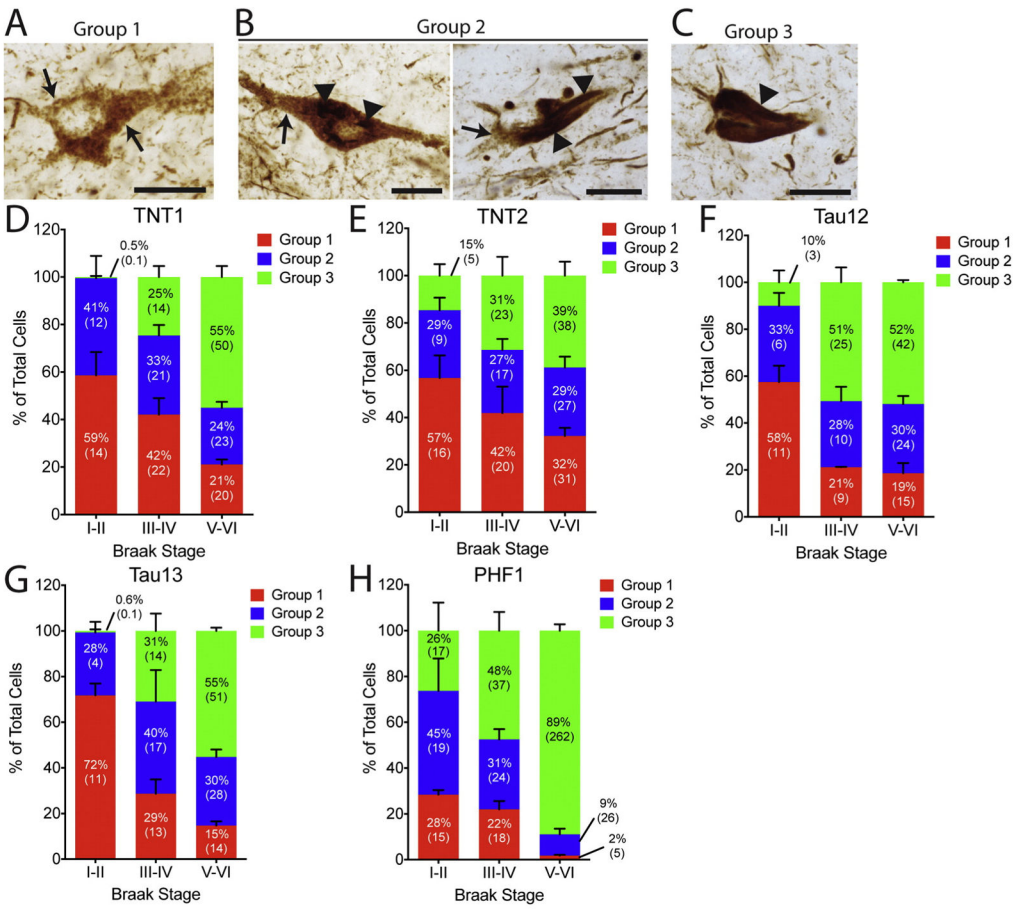

Fig. 5. Percentages of the different phenotypes of tau pathology deposition with N-terminal tau antibodies in human hippocampal tissue across Braak stages

(*A*–*C*) Representative examples of (*A*) a group 1 neuron, (*B*) two group 2 neurons, and (*C*) a group 3 neuron. These cellular phenotypes are established previously (Braak et al., 1994). Group 1 cells are characterized by diffuse granular cytoplasmic staining (arrows), group 2 cells contain diffuse granular staining (arrows) and some discrete regions of more compact inclusions (arrowheads), and group 3 neurons no longer contain diffuse granular staining but contain large compact tangles (arrowhead, i.e., classic NFTs). Scale bars are 25 μm in (*A*–*C*). (*D*–*H*). The percentage of group 1, 2, and 3 cells (reported as the mean of the percents from each case with error bars representing the SEM), with the total number of cells/mm^2 in parentheses (reported as the mean of cell densities from each case), labeled by the (*D*) TNT1, (*E*) TNT2, (*F*) Tau12, (*G*) Tau13, and (*H*) PHF1 antibody are compared between the Braak stages. (*D*) In Braak I–II cases, TNT1 labeled more group 1 and 2 cells compared to group 3 cells. In Braak III–IV cases, TNT1 labeled similar amounts of each phenotype, while in Braak V–VI cases, more group 3 cells were labeled when compared to group 1 and 2 cells. (*E*) TNT2 labeled more group 1 cells compared to group 3 cells, while in Braak III–IV cases, similar amounts of each phenotype were labeled, and in Braak V–VI cases, the majority were group 3 cells. (*F*) In Braak I–II cases, Tau12 labeled more group 1 cells compared to group 2 and 3 cells. In both Braak III–IV and V–VI cases, Tau12 labeled more group 3 cells compared to group 1 and 2 cells. (*G*) Tau13 labeled more group 1 cells

compared to group 2 and 3 cells. Similar proportions of each phenotype were identified with Tau13 in Braak III–IV cases, while in Braak V–VI cases more group 3 cells were labeled when compared to group 1 and 2 cells. (*H*) PHF1 stained similar amounts of all three cell phenotypes in Braak I–II and more group 3 cells compared to groups 1 and 2 in III–IV cases. A dramatic increase in PHF1 labeled group 3 cells was observed in Braak V–VI cases.

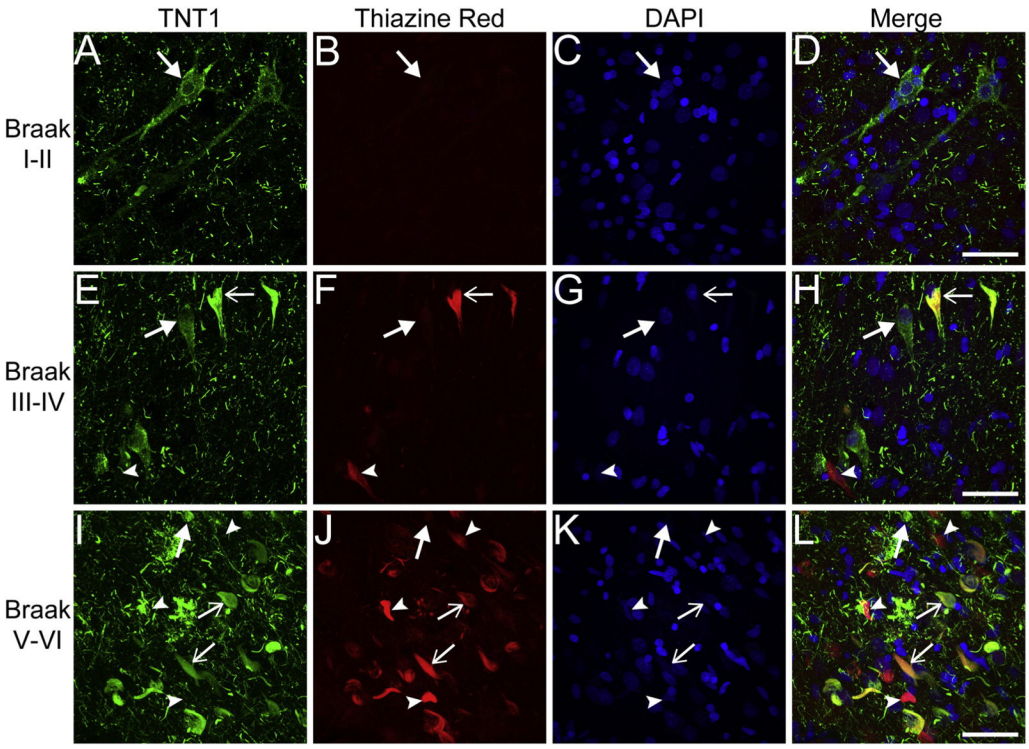

Fig. 6. Multi-label fluorescent stain indicates TNT1 detects early tau pathology in disease

Qualitative assessment of TNT1 reactivity confirmed that PAD exposure occurred in early, pre-tangle pathology, remained in classic NFTs, but was absent in later stage NFTs (e.g. ghost tangles). Representative multi-label fluorescent stain images were capture to show TNT1 (*A*, *E*, *I*; green, a marker of PAD-exposed tau), ThR (*B*, *F*, *J*; red, β-sheet structure present in classic NFTs), and DAPI (*C*, *G*, *K*; blue, nuclei). Merged images are shown in (*D*, *H*, *L*). (*A–D*) TNT1 labeled diffuse pre-tangles in Braak I–II that were ThR negative (solid arrow). (*E–H*) TNT1 identified neurons that are ThR negative (solid arrow) and more compact classic NFTs that are ThR positive (open arrow) in Braak stages III–IV. Occasional late-stage NFTs (e.g. ghost tangles lacking nuclei) were ThR positive and TNT1 negative (solid arrowhead). (*I–L*) TNT1 continued to label ThR-negative structures (solid arrow) in Braak V–VI, as well as more mature ThR-positive NFT inclusions (open arrow). Notably, the vast majority of TNT1-positive threads were ThR negative. Many ThR-positive cells were TNT1 negative and did not have nuclei (i.e., ghost tangles) in the later disease stages (solid arrowhead). Scale bars represent 50 μm.

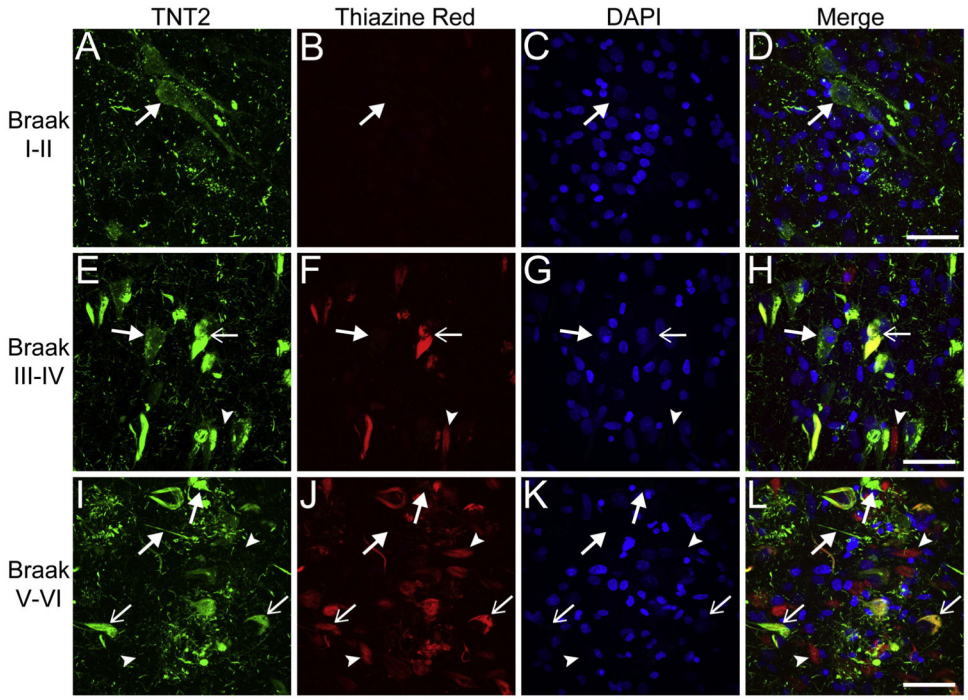

Fig. 7. Multi-label fluorescent stain indicates TNT2 detects early tau pathology in disease

Qualitative assessment of TNT2 reactivity confirmed that PAD exposure occurred in early, pre-tangle pathology, remained in classic NFTs but was absent in later stage NFTs (e.g. ghost tangles). Representative multi-label fluorescent stain images were captured to show TNT2 (*A*, *E*, *I*; green, a marker of PAD-exposed tau), ThR (*B*, *F*, *J*; red, β-sheet structure present in classic NFTs), and DAPI (*C*, *G*, *K*; blue, nuclei). Merged images are shown in (*D*, *H*, *L*). (*A–D*) TNT2 labeled diffuse pre-tangles in Braak I–II that were ThR negative (solid arrow). (*E–H*) TNT2 identified neurons that are ThR negative (solid arrow), as well as more compact classic NFTs that are ThR positive (open arrow) in Braak stages III–IV. Occasional late-stage NFTs (e.g. ghost tangles lacking nuclei) were ThR positive and TNT2 negative (solid arrowhead). (*I–L*) TNT2 continued to label ThR-negative structures (solid arrow) in Braak V–VI, as well as more mature ThR-positive NFT inclusions (open arrow). Like TNT1, the vast majority of TNT2-positive threads were ThR-negative and many of ThR-positive cells were TNT2 negative and did not have nuclei (i.e., ghost tangles; solid arrowhead). Scale bars represent 50 μm.

Table 1

Correlations between Braak stages and group 1, group 2, or group 3 cell phenotypes labeled with TNT1, TNT2, Tau12, Tau13, and PHF1.

Tau antibody	Cell phenotype	% Labeled cells vs Braak stage (r value)
TNT1	Group 1	−0.843*
	Group 2	−0.580
	Group 3	0.953*
TNT2	Group 1	−0.715*
	Group 2	0.053
	Group 3	0.738*
Tau12	Group 1	−0.791*
	Group 2	−0.158
	Group 3	0.791*
Tau13	Group 1	−0.896*
	Group 2	0.105
	Group 3	0.953*
PHF1	Group 1	−0.896*
	Group 2	−0.843*
	Group 3	0.843*

* $p < 0.05$ in Spearman rank correlation test.